

Colliding-pulse passive harmonic mode-locking in a femtosecond Yb-doped fiber laser with a semiconductor saturable absorber

Y. Deng, M. W. Koch, F. Lu, G. W. Wicks, W. H. Knox

The Institute of Optics, University of Rochester, Rochester, NY 14627-0186

Tel: 585-275-2323, Fax: 585-244-4936,

yideng@optics.rochester.edu

Abstract: We demonstrate a passive harmonic mode-locked femtosecond Yb-doped fiber laser employing a semiconductor saturable absorber in a colliding-pulse configuration. 380-fs pulses at 605 MHz repetition rate with >60 dB supermode suppression is achieved.

©2004 Optical Society of America

OCIS codes: (060.2320) Fiber optics amplifiers and oscillators; (320.7090) Ultrafast lasers

References and links

1. V. Cauterets, D. J. Richardson, R. Paschotta, and D. C. Hanna, "Stretched pulse Yb³⁺ silica fiber laser," *Opt. Lett.* **22**, 316 (1997).
2. L. Lefort, J. H. V. Price, D. J. Richardson, G. J. Spühler, R. Paschotta, U. Keller, A. R. Fry, J. Weston, "Practical low-noise stretched-pulse Yb³⁺-doped fiber laser," *Opt. Lett.* **27**, 291 (2002).
3. F. Ö. Ilday, J. R. Buckley, H. Lim, F. W. Wise, and W. G. Clark, "Generation of 50-fs, 5-nJ pulses at 1.03 μ m from a wave-breaking-free fiber laser," *Opt. Lett.* **28**, 1365 (2003).
4. F. Ö. Ilday, J. Buckley, L. Kuznetsova, and F. W. Wise, "Generation of 36-femtosecond pulses from a ytterbium fiber laser," *Opt. Express* **11**, 3550 (2003).
<http://www.opticsexpress.org/abstract.cfm?URI=OPEX-11-26-3550>
5. J. Limpert, T. Schreiber, T. Clausnitzer, K. Zöllner, H.-J. Fuchs, E.-B. Kley, H. Zellmer, and A. Tünnermann, "High-power femtosecond Yb-doped fiber amplifier," *Opt. Express* **10**, 628 (2002).
<http://www.opticsexpress.org/abstract.cfm?URI=OPEX-10-14-628>
6. S. Chu, T. Liu, C. Sun, C. Lin, and H. Tsai, "Real-time second-harmonic-generation microscopy based on a 2-GHz repetition rate Ti:sapphire laser," *Opt. Express* **11**, 933-938 (2003).
<http://www.opticsexpress.org/abstract.cfm?URI=OPEX-11-8-933>
7. C. Schaffer, J. Garcia and E. Mazur, "Bulk heating of transparent materials using a high repetition-rate femtosecond laser," *Appl. Phys. A*, **76**, 351 (2003).
8. C. X. Yu, H. A. Haus, E. P. Ippen, W. S. Wong and A. Sysoliatin, "Gigahertz-repetition-rate mode-locked fiber laser for continuum generation," *Opt. Lett.* **25**, 1418 (2000).
9. N. H. Bonadeo, W. H. Knox, J. M. Roth, K. Bergman, "Passive harmonic mode-locked soliton fiber laser stabilized by an optically pumped saturable Bragg reflector," *Opt. Lett.* **25**, 1421 (2000).
10. Thomas F. Carruthers, Irl N. Duling III, "10-GHz, 1.3-ps erbium fiber laser employing soliton pulse shortening," *Opt. Lett.* **21**, 1927 (1996).
11. T. Carruthers, I. Duling, and M. Dennis, "Active-passive modelocking in a single-polarization Erbium fiber laser," *Electron. Lett.* **30**, 1051 (1994).
12. M. Guina and O. G. Okhotnikov, "Harmonic mode locking by synchronous optical pumping of a saturable absorber with the residual pump," *Opt. Lett.* **28**, 358 (2003).
13. J. F. Martins-Filho, E. A. Avrutin, C. N. Ironside and J. S. Roberts, "Monolithic multiple colliding pulse mode-locked quantum-well lasers: experiment and theory," *IEEE J. Selected Topics in Quantum Electron.*, **1**, 539, (1995).
14. O. G. Okhotnikov, M. Guina, "Colliding-pulse harmonically mode-locked fiber laser," *Appl. Phys. B* **72**, 381 (2001).
15. Rüdiger Paschotta, Johan Nilsson, Anne C. Tropper, and David C. Hanna, "Ytterbium-doped fiber amplifiers," *IEEE J. Quantum Electron.*, **33**, 1049, (1997).
16. A. Galvanauskas, "Mode-scalable fiber-based chirped pulse amplification systems," *IEEE J. Selected Topics in Quantum Electron.*, **7**, 504, (2001).
17. W. H. Knox, "In situ measurement of complete intracavity dispersion in an operating Ti:sapphire femtosecond laser," *Opt. Lett.* **17**, 514 (1992).

18. Q. Ye, C. Xu, X. Liu, W. H. Knox, et. al., "Dispersion Measurement of Tapered Air-Silica Microstructure Fiber by White-Light Interferometry", *Appl. Opt.*, **41**, 4467 (2002).
19. S. Fleming and T. Whitley, "Measurement and analysis of pumpdependent refractive index and dispersion effects in erbium-doped fiber amplifiers," *IEEE J. Quantum Electron.* **32**, 1113 (1996).
20. Y. Deng and W. H. Knox, "Self-starting passive harmonic mode-locked femtosecond Yb³⁺-doped fiber laser at 1030nm," *Opt. Lett.* **29**, 2121 (2004).
21. W. H. Knox, R. L. Fork, M. C. Downer, D. A. B. Miller, D. S. Chemla, C. V. Shank, A. C. Gossard and W. Wiegmann, "Femtosecond Dynamics of Resonantly Excited Excitons in Room Temperature GaAs Quantum Wells," *Phys. Rev. Lett.* **54**, 1306 (1985).
22. L.E. Nelson, D.J. Jones, K. Tamura, H.A. Haus, E.P. Ippen, "Ultrashort-pulse fiber ring lasers," *Appl. Phys. B* **65**, 277 (1997).
23. Y. Deng and W. H. Knox, "Self-starting passive harmonic mode-locked femtosecond Yb³⁺-doped fiber laser at 1030nm," in *Conference on Lasers and Electro-Optics (CLEO) 2004*, paper CThK2.
24. S. M. Kelly, "Characteristic sideband instability of periodically amplified average soliton," *Electron. Lett.* **28**, 806, (1992).

1. Introduction

In recent years, ytterbium-doped fibers as gain media have attracted great interest because of their broad gain bandwidth, large saturation fluence, high optical pumping efficiency and scalability afforded by cladding pumping technology [1-5]. The first femtosecond mode-locked Yb-doped fiber laser was reported in 1997 [1]. Later, low-noise mode-locking operation was demonstrated in a stretched-pulse Yb-doped fiber laser using a grating-stabilized telecommunications-qualified diode as the pumping source [2]. Recently, a wave-breaking-free Yb-doped fiber laser producing pulses width as short as 36 fs duration and 5 nJ of pulse energy has been reported [3,4], and a high repetition rate femtosecond Yb-doped fiber amplifier with up to 17 W average output power was reported using cladding-pumped Yb:fibers [5].

Femtosecond laser sources with higher repetition rates have certain advantages in many applications such as: biological imaging [6], micro-machining [7] and telecommunications [8,9]. The fundamental repetition rates of fiber lasers are usually less than 100 MHz due to their long fiber lengths. Actively harmonic mode-locked fiber lasers can provide high repetition rate pulses, however in the Kuizenga-Siegman limit, the pulse widths are much longer than those obtained by passive mode-locking. Even with soliton pulse shortening, actively mode-locked fiber lasers operate in the picosecond regime [10]. In order to achieve high repetition rates with femtosecond pulses, various synchronizing schemes have been demonstrated on passive harmonic mode-locked fiber lasers. These include using an amplitude modulator [11], a phase modulator [8], an optically pumped semiconductor saturable Bragg reflector (SBR) [9] and a semiconductor saturable absorber modulated with residual pump light [12]. Significant supermode suppression is achieved along with <500 fs pulses [8,9], however all these schemes rely on complex electronic and RF components to provide regenerative stabilization.

Colliding pulse harmonic mode-locking has been used to scale up the repetition rate in passive mode-locked quantum well semiconductor lasers [13]. Recently, colliding-pulse harmonic mode-locking has been demonstrated in an Er-doped fiber laser producing picosecond pulses at 200 MHz repetition rate with 50 dB supermode suppression [14]. The maximum achievable active-ion concentrations for Yb doping in the fiber core can be significantly higher than for Er doping, thus enabling one to reach very high optical gain in a relatively short length of a fiber [15,16]. This leads to a shorter cavity with higher fundamental repetition rates for Yb-doped fiber lasers. Further exploiting the colliding-pulse harmonic mode-locking scheme in Yb-doped fiber laser for the development of a higher repetition rate femtosecond laser would be advantageous for many applications.

2. Experimental setup

In this paper, we report a colliding-pulse harmonic mode-locked Yb-doped fiber laser producing 380-fs pulses at 605 MHz repetition rate with >60 dB supermode suppression. The experimental setup is shown in Fig. 1. The laser is pumped by a grating-stabilized telecommunications-qualified 976-nm laser-diode with 400 mW maximum output power. The total length of the fiber section is 3.5 m including 34 cm of highly-doped Yb:fiber (NA=0.13, Core Diameter=6.3 μm) and 3.16 m Lucent 980-nm coupler fiber. The doping density of the Yb:fiber is ~24000 ppm by weight (INO, inc.). The maximum small-signal gain at 1030nm is estimated to be ~150dB/m when pumped at 976nm [15]. In order to increase the intracavity nonlinearity, the gain fiber is located in the front part of the fiber section. A 600-line/mm diffraction grating pair is used to compensate for the normal dispersion of the fiber. The slant separation of the grating pairs is 12 cm with beam incident at a 30° angle with respect to the grating normal. The double pass second-order dispersion introduced by the grating pair is -0.186 ps^2 . The round trip second-order dispersion is measured to be -0.07 ps^2 by the Frequency Domain Dispersion (FDD) technique [17]. A positive dispersion of $27 \text{ ps}^2/\text{km}$ in the Lucent 980-nm coupler fiber is measured with broadband interferometric method [18]. This generally agrees with the intracavity dispersion measurement, considering we neglect the dispersion contribution from the isolator, the pump-induced change in the refractive index of the gain fiber [19] and the nonlinearity effects. The fundamental repetition rate of the laser is 43.2 MHz. An auxiliary colliding-pulse arm is introduced into the main cavity by using a polarizing beam splitter (PBS) ($T_p/T_s > 1000$). Two aspheric lenses ($f=15.36\text{mm}$, NA=0.16) are used to form a diffraction-limited focus. A semiconductor saturable absorber (SSA) is placed between the two lenses near the focus position, allowing us to vary the spot size and therefore the effective saturation fluence of the SSA. The quarter wave plate (QWP) after the focusing unit is used to transform the incoming vertical linearly polarized beam into a clockwise circularly polarized beam, and then transform the reflected counter-clockwise circularly polarized beam back to a horizontal linearly polarized beam. One advantage of this setup is that any residual reflection from the SSA will be effectively blocked by the PBS, thus avoiding the deleterious effects of spurious reflections on passive mode-locking. The saturation of the semiconductor absorption is enhanced when the incoming and outgoing pulses collide in the SSA. By adjusting the end high reflector (HR) position so that the optical path of segment L_S is exactly one sub-multiple of the total cavity length, only one specific harmonic of the laser cavity is so enhanced. In this paper, we set L_S as 1/14 of the total cavity length.

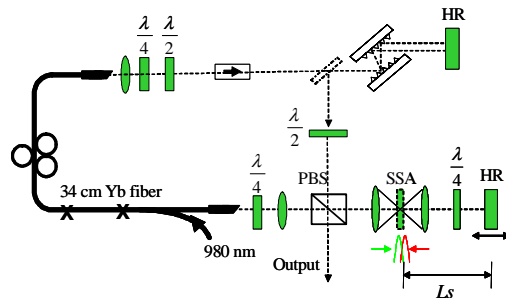


Fig. 1 The experimental configuration, L_S is set to be 1/14 of the total cavity length.

3. Properties of the semiconductor saturable absorber (SSA)

The SSA consists of 500 nm of $\text{In}_x\text{Ga}_{1-x}\text{As}$ grown by molecular beam epitaxy (MBE) on a 500 μm thick semi-insulating GaAs substrate at 430°C at a growth rate of 1 micron/hr. Growth at 430°C results in the intentional incorporation of defects, which shorten the carrier recombination time. The indium fraction of $x \sim 15\%$ places the bandgap energy at $\sim 1.19 \text{ eV}$,

which corresponds to a wavelength of ~ 1040 -nm. The sample is anti-reflection coated on both sides at 1030 nm. Figure 2(b) shows the transmission spectrum of the SSA measured with a Perkin-Elmer Lambda 900 spectrophotometer.

A standard pump-probe experiment is performed to investigate the saturation dynamics and modulation depth of the SSA. The experimental setup is shown in Fig. 2(a). The source for the experiment is a homebuilt mode-locked Yb-doped fiber laser with an integrated fiber amplifier [20], producing 260-fs pulses at a 58 MHz repetition rate at round 1030 nm. The average power of the pump beam is set to ~ 9 mW, which corresponds to 0.15nJ pulse energies. An aspheric lens with 0.16 NA is used to focus the pump beam to a ~ 10 μm diameter spot, roughly reproducing the intracavity conditions of the present laser.

The pump-probe signal is shown in Fig. 2(c). An initial ~ 200 -fs fast component in the transmission response arises from the thermalization of the near-bandedge-excited carriers [21]. The ~ 20 ps slow component is caused by the nonradiative recombination of the excited carriers. The measured modulation depth on the transmission of the SSA is $\sim 3\%$.

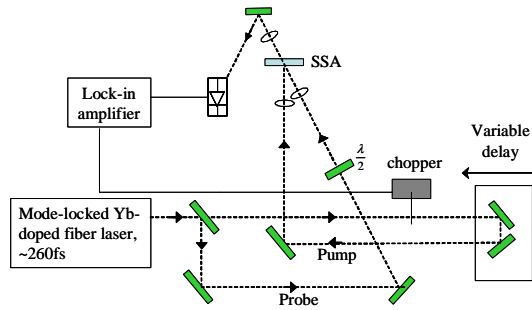


Fig. 2. (a) The configuration of the pump-probe experiment.

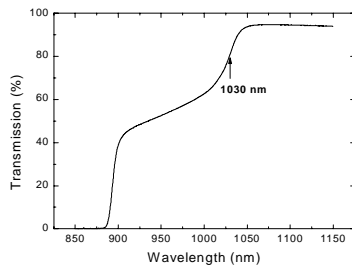


Fig. 2. (b) The transmission spectrum of the SSA.

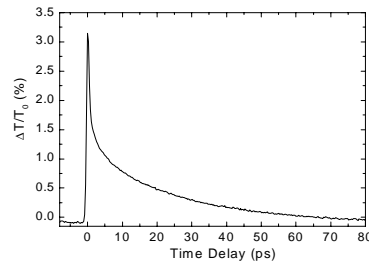


Fig. 2. (c) Transmission response of the SSA measured by the pump-probe

4. Experimental result

The threshold pump power of the laser cavity is ~ 20 mW. As shown Fig. 1, the laser can operate in two different regimes: nonlinear polarization rotation (NPR) modelocking, and semiconductor saturable absorption modelocking. With no SSA in the cavity, the laser can be mode-locked with the NPR effect by adjusting the waveplates inside the cavity. In this case, the pump power threshold for self-starting modelocking is ~ 150 mW, critically depending upon the setting of the waveplates. By introducing the SSA into the cavity, stable mode-locking (without any Q-switching) is achieved with pump power as low as 50mW, and in this mode the self-starting is not critically dependent on the waveplate settings.

4.1 Fundamental modelocking conditions

The mode-locking effect, as the result of NPR, can be minimized by adjusting the waveplates to maximize the laser output when the laser is operating just above the threshold. At this point, the mode-locking is dominated by the saturation dynamics in the SSA. The laser tends to run in fundamental mode-locking with the spectrum shown in Fig. 3(a). The fundamental mode-locking is energetically more favorable, since the SSA should be more deeply saturated by one large pulse than by the colliding of multiple small pulses. No multiple pulsing or bunching is observed even when the laser is pumped with the full pump power. More than 120-mW of average power, ~2.8 nJ pulse with ~500-fs pulse widths is achieved directly from the laser oscillator.

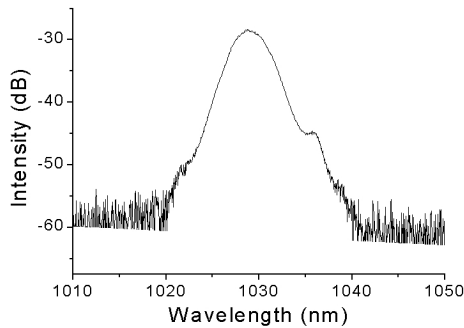


Fig. 3. (a) Optical spectrum of the fundamental mode-locking caused by the SSA.

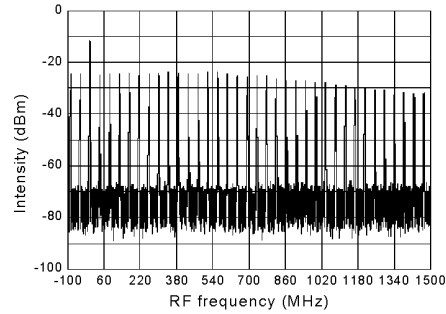


Fig. 3. (b) RF spectrum of the fundamental mode-locking caused by the SSA.

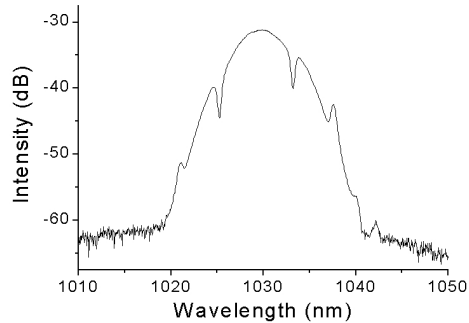


Fig. 3. (c) Optical spectrum of the 14th harmonic mode-locking.

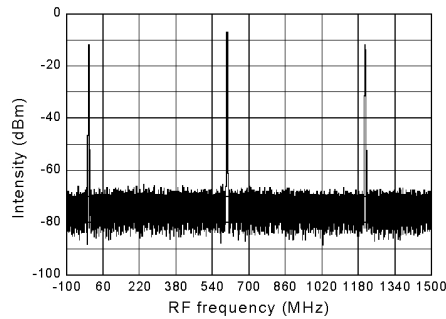


Fig. 3. (d) RF spectrum of the 14th harmonic mode-locking at 605 MHz, the supermode suppression is >60 dB.

4.2 Harmonic modelocking conditions

Stable harmonic mode-locking conditions are achieved as a result of the interplay of the two co-existing mode-locking mechanisms. As one adjusts the linear birefringence bias by tuning the waveplates, the effective saturation threshold of SAM effect is changed. Over-saturation of the effective saturable absorber results in multiple pulse operation [22]. When the pump power and the setting of the waveplates is right, these multiple pulse trains reach a nominally equal spacing in <0.1 s. The supermode spikes in the RF spectrum are strongly suppressed, as shown in Fig. 3(d). We achieve over 60 dB of supermode suppression at the 14th harmonic with 605 MHz repetition rate and ~6 mW of average output power. We find that the supermode suppression ratio is very sensitive to the distance between the SSA and the end HR, strongly suggesting that the colliding pulse effect strengthens the action of the harmonic operation. As shown in Fig. 3(a) and (c), the spectral width is broader in harmonic mode-locking due to the stronger pulse shaping effect when NPR is contributing significantly. The pulse spectrum also develops some structures as the result of the energy coupling between the pulses and the dispersive wave in the cavity [23].

The autocorrelation trace of the pulse at 14th harmonic mode-locking shown in Fig. 4(a) is measured by a Two-Photon Absorption (TPA) interferometric autocorrelator employing a photomultiplier tube (PMT) with cutoff wavelength at around 650 nm (Hamamatsu 1P21). The FWHM of the autocorrelation trace is ~650 fs. The FWHM of the pulse is estimated to be ~380 fs. For the intracavity dispersion of -0.07 ps^2 , the laser is operating in soliton regime [22]. The stretching ratio is estimated to be less than 3. As the output port is located right after the grating pair, a small amount of negative chirp is expected. The trace on the oscilloscope shows a stable pulse train at 605 MHz as shown in Fig. 4(b). The harmonic mode-locking is very robust, exhibiting a stable operation that lasts for several days without any readjustment.

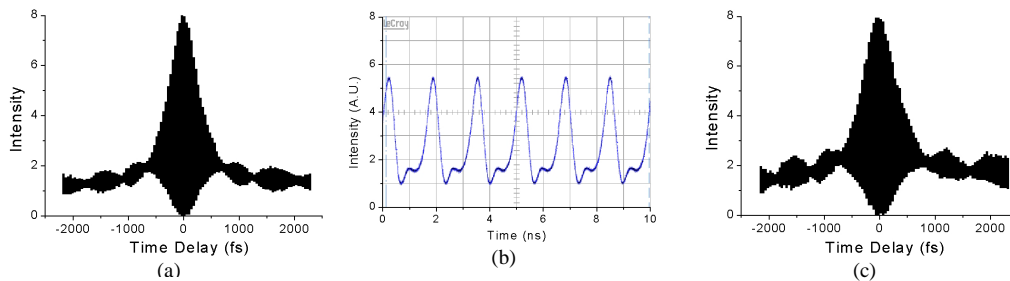


Fig. 4. (a) The interferometric auto-correlation of the pulse at 14th harmonic, the FWHM of the trace is ~650-fs, the FWHM of the pulse is estimated to be ~380-fs; (b) The pulse train of the 14th harmonic mode-locking at 605 MHz; (c) Cross-correlation between adjacent pulses, the FWHM of the trace is ~820-fs.

We also performed an optical cross-correlation between adjacent pulses by introducing a one-pulse delay in one arm of the interferometric autocorrelator. Figure 4(c) shows the typical cross-correlation trace. It has ~820-fs FWHM, broadened by a factor of 1.26 compared with the auto-correlation trace. The fact that we were able to get an interferometric cross-correlation trace between consecutive pulses indicates that there is certain phase correlation between them established via the cross-saturation effect in the SSA. It has to be mentioned that this established phase relation is not stable in the long term. Destabilization will cause disappearance of the interferometric cross-correlation trace. We are investigating the stabilization mechanisms for this phase correlation between pulses. Passive harmonic mode-locking with 45~50 dB supermode suppression has been reported in a laser with similar design [20,24], but without the colliding-pulse configuration. Timing jitter measurement shows that the pulse train has ~14 ps of timing jitter. With that laser, no interferometric cross-correlation trace, as Fig. 4(c), has been observed. Therefore, we attribute the significant pulse-to-pulse timing jitter reduction along with the >60 dB supermode suppression to the cross-saturation of the two colliding pulses on the SSA.

There is a major difference between our scheme and the one reported in [14]. When the laser is operating in the harmonic mode-locking mode, as the SAM effect of NPR is dominant, the SSA acts principally as a harmonic mode-locking stabilizer. By making use of the SAM effect of NPR, we can get shorter pulse widths and more stable pulse trains. No couple cavity effect is observed in the laser, because any residual reflection from the SSA will be effectively blocked by the high distinction ratio PBS ($T_p/T_s > 1000$), also extra care has been taken to avoid residual reflection from the SSA back into the laser cavity by tilting it in a small angle off the optical axis.

In conclusion, we have shown that a semiconductor saturable absorber operated in transmission mode can be incorporated in a colliding-pulse laser configuration in combination with strong nonlinear polarization rotation modelocking. Using this scheme, we demonstrate a colliding-pulse harmonic mode-locked Yb-doped fiber laser producing ~380-fs pulses at 605 MHz repetition rate with >60 dB of supermode suppression.